(4)

Final Report

Contract #N00014-88-C-2033

"Pigtailed Single-mode Diode Lasers"

Issued by

Naval Research Laboratory

Washington, D.C. 20375-5000

Dr. Norman Kwong

Ortel Corporation

2015 W. Chestnut St., Alhambra CA, 91803

Contract Period:

88 SEP 30 - 89 APR 30

TABLE OF CONTENTS

1 Theoretical Analysis of Coupling to a Single Mode Fiber

1.1 Introduction

In choosing a scheme for single mode fiber coupling, the final evaluation should of course be based on an experimental comparison between the alternatives. However, such an evaluation will generally not reveal the essential limitations of any scheme. While the possible sources of less than ideal performance are well known, their relative significance is not so obvious. It is clear that in order to make significant improvements in the state of fiber coupling technology, the relevant limitations must be clarified in order to guide further efforts in fruitful directions. As such, we have conducted an analysis of several aspects of the fiber coupling problem which is presented here. Preliminary to the consideration of any particular system, the importance of the zeroth and first order properties of the coupling system are briefly discussed. To go beyond this, the higher order aberrations of the optical coupling system must be included in the analysis. To do this, an algorithm to calculate the mode coupling performance of any optical system has been developed using the ray tracing features of an optical design program. This algorithm is described along with the results of an analysis of coupling with graded index lenses which have been found to work well experimentally.

1.2 Light Source and Fiber Modes

Prior to any consideration of mode coupling, the modes of the light source and fiber must be established. Following convention, we

assume both the light source and fiber modes to be Gaussian beams in the far field. Thus their electric field amplitudes, $E(x,y)$, in the far field are given by [1]:

$$|E(x,y)| = \left(\frac{\ln 2}{\pi L^2 \tan\left(\frac{\theta_x}{2}\right)\tan\left(\frac{\theta_y}{2}\right)}\right)^{1/2} \exp\left[-\frac{\ln 2}{2}\left(\left(\frac{x}{L\tan\frac{\theta_x}{2}}\right)^2 + \left(\frac{y}{L\tan\frac{\theta_y}{2}}\right)^2\right)\right] \quad (1)$$

where θ_x and θ_y are the far field intensity full width at half maximum (FWHM) angles, and L is the distance along the optical axis from the beam waist. The wavefronts in the far field are assumed to be spherical and centered on the beam waist. This is true in general for any field confined to a small area with a planar wavefront at some plane (i.e., an index-guided laser diode facet or fiber end) as is easily shown by a far field approximation of the Rayleigh-Sommerfeld diffraction formula [2].

The laser and SLD we used in experiments had far field angles which were measured to be 15° and 50° FWHM in x and y respectively. These values have to be corrected slightly for use in Eqn. 1 since the measurement system measures intensity versus angle at a fixed distance and with the detector always facing the source while the angles defined in Eqn. 1 are based on intensity in a fixed x-y plane and measured normal to this plane. With this correction, θ_x and θ_y are 14.7° and 42.7° respectively.

The fiber mode is evaluated from the following expression for the Gaussian beam waist, ω_0, of a single mode fiber with core radius a [3]:

$$\frac{\omega_0}{a} = 0.65 + \frac{1.619}{V^{3/2}} + \frac{2.879}{V^6} \qquad (2)$$

where V is the normalized frequency defined as $V = 2\pi \cdot NA \cdot a/\lambda$ and NA is the numerical aperture of the fiber. For a single mode fiber with NA=0.11 and a wavelength of $\lambda = 0.83\mu m$, the fiber mode has a far field angle of 5.8° FWHM.

1.3 Zeroth and First Order Considerations

Before considering aberrations, it is useful to look at the zeroth and first order aspects of the problem. This will help clarify where major improvements could be made, and also what sort of peak performance might be ideally expected.

The zeroth order light collecting capability can be a problem in some coupling systems since the typically large far field angles of laser diodes require high numerical aperture optics for complete collection. The model PCH GRIN lenses, with an NA of 0.60, are well suited to laser diodes in this regard. For the laser diodes we are using, these lenses capture >99% of the far field intensity pattern. As will be discussed, however, high aberrations near the lens edge significantly reduce the useful aperture.

As an upper limit to aberration-free performance, we consider the ideal coupling between circular and elliptic Gaussian beams with perfect phase matching (i.e., the beams have spherical wavefronts with the same center). The two sources of non-optimal (< 100%) coupling then are mismatch in the beam spot sizes, and incompatibility in their shapes. The power coupling efficiency can be evaluated analytically in this case with the result [4]:

$$\eta = 4/\left[\left(\frac{\beta_x}{\beta}+\frac{\beta}{\beta_x}\right)\left(\frac{\beta_y}{\beta}+\frac{\beta}{\beta_y}\right)\right] \tag{3}$$

. The parameters β, β_x, β_y are just the $\tan(\theta/2)$ values from Eqn. 2 for the circular beam, and the x,y axes of the elliptical beam respectively. For a given β_x, β_y, the optimum value of the circular beam parameter, β, is:

$$\beta_{opt} = \sqrt{\beta_x \beta_y}. \tag{4}$$

In Fig. 1, we plot Eqn. 3 as a function of the spot size matching parameter $\beta/\sqrt{\beta_x\beta_y}$ for various degrees of ellipticity (i.e., β_y/β_x or β_x/β_y). Although it is generally asserted that perfect coupling can not be achieved between circular and elliptical beams, it is seen that even for an ellipticity of 2, the actual reduction from the optimum-both beams circular- is not very serious and a peak coupling of about 90% is possible.

The variation in coupling with respect to the abscissa reflects the importance of matching spot sizes or equivalently, far field angles. The matching of the typically wide laser beam angle to the narrow

fiber mode angle is accomplished through the optical system magnification, M. To first order, the beam parameters before (primed) and after (unprimed) the lens system are simply related by:

$$\tan(\theta_x/2) = \frac{1}{M}\tan(\theta_x'/2) \qquad \tan(\theta_y/2) = \frac{1}{M}\tan(\theta_y'/2) \tag{5}$$

Combining these relations with Eqn. 4 defines an optimum magnification:

$$M_{opt} = \frac{\sqrt{\tan(\theta_x'/2)\tan(\theta_y'/2)}}{\tan(\theta/2)} \tag{6}$$

With this definition, the abscissa of Fig. 1 may also be considered as the quantity M/M_{opt}. Thus it is seen that operating close to optimal magnification is important for high coupling. For example, in order to attain 90% of the optimum coupling, the magnification must be within a factor of 1.4 of the optimum magnification.

1.4 Aberrations-Ray Tracing Algorithm

In order to accurately calculate the coupling performance of an optical system, one must include the aberrations of the system. Rather than developing an analytic solution based on limited series expansions of the aberrations, we have chosen to utilize the powerful ray tracing analysis features of a commercial optical system design program (Super-OSLO). Since these ray tracing techniques are based on geometrical optics, some care must be taken in incorporating these results into the calculation of mode coupling which is inherently beyond the scope of a completely geometrical optics description.

A single graded index (GRIN) lens coupling system is shown in Fig. 2 with arbitrary input and output planes A and B respectively. The calculation of mode coupling necessarily involves evaluating an overlap integral between the source field and the field distribution of the fundamental fiber mode. However, this integral need not be evaluated at the fiber facet, but may be evaluated at any plane in the optical system. We can then use this flexibility to enable the valid use of ray tracing and evaluate the full effect -- including aberrations -- of the optical system on the source field. Specifically, since the region between planes A and B is far from any focus points (beam waists), the field propagation is well described by geometrical optics and ray tracing may be used to evaluate the source field at the plane B from a given field at A. The coupling efficiency, η, is then found by numerically calculating the following[5] at plane B:

$$\eta = \frac{\left| \int\int dx\,dy\, E_1(x,y) E_2^*(x,y) \right|^2}{\int\int dx\,dy |E_1|^2 \int\int dx\,dy |E_2|^2} \tag{7}$$

where $E_1(x,y)$ and $E_2(x,y)$ are the source and fiber fields.

In order to propagate the source field through the optical system, a finite aperture at plane A is divided into a rectangular grid-denoted by the indices (i,j)-and the field at each point is then propagated to plane B by ray tracing. For our calculations we used a grid of 60×60 points, although symmetry usually means only one or two quadrants need actually be evaluated which reduces computation time. In general,

one must describe the field at A in terms of an initial phase and ray direction (phase gradient) at each point in order to perform the appropriate ray trace. However, since the far field of the laser output has spherical wavefronts, all rays can be traced as if originating from a single point at the beam waist. Also, the optical path length measured from this point will determine the source field phase at plane B. The optical design program Super-OSLO is used to trace these rays, and outputs the position-x(i,j) and y(i,j)-as well as the optical path length-OPL(i,j)-of each ray at plane B.

The ray positions x(i,j),y(i,j), define a new grid at plane B which is not necessarily square due to aberrations of the lens system. If rays cross before reaching plane B, then the relative ordering of the rays is changed which greatly complicates the problem. In order to avoid this, we restrict the aperture at plane A to a size small enough to preclude such rays. This does not artificially reduce the coupling efficiency since from a physical point of view these rays typically miss the fiber altogether. If chosen too small, the aperture *would* affect the results since it would neglect rays which significantly contribute to the coupling. Therefore, we choose an intermediate size aperture which prevents ray crossings before plane B, but still allows rays which are sufficiently aberrated that they miss the fiber. That these rays do not contribute to the coupling integral was verified by checking that the phase difference from the spherical fiber wavefront is several waves and is changing very quickly with radial position.

For the laser and GRIN lens described here, we find that this aperture typically collects only about 90% of the laser power so the lens aberrations significantly limit the useful area to much less than the numerical aperture indicates. As a more definite indicator of this limitation, we find that the radius at which the phase mismatch has become a full wave only captures about 75% of the total laser power.

In order to do integrals in the B plane, we associate an area, $a_B(i,j)$, with each grid point equal to the average of the four grid "boxes" surrounding that point. This then accounts for local magnification variations while preserving the total area of the grid. The overlap integral from Eqn. 7 is then approximated as :

$$\int\int dx\,dy\,E_{1B}E_{2B} \approx \sum_{i,j} E_{1B}(i,j)E^{*}_{2B}(i,j)a_B(i,j) \qquad (8)$$

where the subscript B denotes evaluation at the plane B. The field E_{2B} is given by the analytic expression (Eqn. 2) for the fiber mode evaluated at the point {x(i,j), y(i,j)}. The field $E_{1B}(i,j)$ is the propagation of $E_{1A}(i,j)$ which is given by the analytic expression for the laser mode at plane A. The phase change on propagation is easily derived from the ray trace path length data; however, there is also an amplitude change which has been incorrectly treated as a uniform magnification in other work in the literature [6]. Instead, the distortion of the grid implies a *nonuniform* magnification which will distort the shape of the field amplitude distribution. To properly account for this, we impose conservation of the optical power flux in each ray bundle in

accord with well known results from geometrical optics[7]. Since intensity is proportional to the square of the field, the field of each ray must scale inversely as the square root of the area associated with that ray. Thus the field magnitude propagates along ray (i,j) as:

$$|E_{1B}(i,j)| = |E_{1A}(i,j)|\sqrt{a_A(i,j)/a_B(i,j)} \qquad (9)$$

Inserting this in the summation of Eqn. 8, the coupling efficiency-Eqn. 7-is numerically evaluated as:

$$\eta \approx \left| \sum_{i,j} |E_{1A}(i,j)| \exp\left(j\frac{2\pi}{\lambda} OPL(i,j) \right) E^{*}_{2B}(i,j) \sqrt{a_A(i,j)\, a_B(i,j)} \right|^2, \qquad (10)$$

where E1A, E2B are normalized at their respective planes, and OPL(i,j) is the path length of ray (i,j) measured from the source point. The areas $a_A(i,j)$ are actually all the same due to choosing a square input grid.

Once a set of rays has been traced, the effects of varying the laser far field, the fiber far field, and the fiber facet position can all be quickly calculated by making appropriate changes to the functions E1A and E2B. In this manner, we typically zero in on a best focus position for the fiber, starting with a geometrical optics initial guess. We then investigate the coupling tolerance with respect to movement about this point along the longitudinal and two transverse axes. Finally, the optical system itself can be readily changed and can include a very broad range of components due to the convenient lens entry features of the Super OSLO program.

2 Fiber Coupling with GRIN Lenses:Experiment and Calculations

2.1 Experimental Set-up

The experimental set-up is shown in Figs. 3(a) and 3(b). The light source is a GaAs device which can be operated in either SLD or laser mode [7]. Fig. 4 is a schematic diagram of the light source we used in the experiment. The light versus injection current characteristics is shown in Fig. 5, curve (a). The device operates in the superluminescent mode for the current less than 35 mA. When the current is higher than 35 mA, the absorber is bleached through and the device becomes a multimode laser. The spectral characteristics of the light source in both the SLD and the laser mode are shown in Fig. 6. The light output from the device was coupled to a single mode polarization preserving fiber (SMPPF) through the GRIN lens as shown in Fig. 3(b). The light versus current curves before and after fiber coupling are shown in Fig. 5. The fiber coupling efficiency for the SLD and laser mode are measured to be 17% and 22%, respectively. The far-field pattern of the light source at various currents are shown in Figs. 7(a) and 7(b). The far-field full widths at half-maximum are 15° and 50° for scans parallel and perpendicular to the junction plane, respectively. The far-field pattern of the SLD and the laser are basically the same.

Experimentally, we also confirm that the optical spectrum before and after fiber coupling is basically the same. Therefore the difference in fiber coupling efficiency cannot be explained by chromatic dispersion

of the lens or any wavelength dependent effect. We suspect that the light output from the SLD contains both guided modes and radiation modes (non-guided modes). The radiation modes have much less coupling efficiency than the guided modes. On the other hand, the output from a laser is confined to guided modes.

2.2 Graded Index Lens

Presently, a major factor limiting the accuracy of the calculations is the lack of data for accurately characterizing the GRIN lens. In particular, the actual index variation must be known in order to account for the lens aberrations. The general form of the radial index variation is written as[9]:

$$n^2(r) = n_0^2[1 - (gr)^2 + h_4(gr)^4 + h_6(gr)^6 + h_8(gr)^8] \qquad (4)$$

While the coefficients n_0 and g are supplied by the manufacturer, the higher order h coefficients are not, though they are crucial to evaluating the lens aberrations. Measurements of these coefficients have been reported for some lenses but not for the PCH model lens which we are using. Based on such measurements of some similar lenses, we chose an estimated value for h_4 which yields results in good agreement with image position specifications supplied by the manufacturer, and also compensates well the spherical aberration of the curved lens surface which was the original intent of this surface. Results of calculations using this model for the GRIN lens are referred to as the "low aberrations" case since h_6 and h_8 equal zero. This model has unrealistically good performance as shown by the ray trace diagram

of Fig. 2 and so we also present results using best estimate values for h_0 and h_8 based on the available data in the literature. While probably not an accurate representation of the actual lens, these models do demonstrate the nature of the effects of the higher order aberrations.

2.3 Maximum Coupling Efficiency and Tolerances

In addition to the absolute coupling efficiency, a primary concern for manufacturing is the tolerance of the coupling to the various alignment positions of the laser, lens, and fiber. Figures 8, 9, and 10 show the variation in coupling efficiency as the fiber end is moved in the x, y, and z directions respectively, relative to the position of maximum coupling. The calculated curves in these figures use the low aberration model and so the absolute coupling efficiencies are higher than measured. However, the tolerances are quite similar in terms of the relative coupling change for a given change in fiber position. The tolerance in the y-direction is more sensitive due to the smaller beam waist normal to the diode junction plane. The experimental coupling of the SLD is not much less than that of the laser indicating that the spatial coherence of the SLD is very good. We also note that the sensitivities to transverse displacement are similar for the laser and SLD.

Figures 11, 12, and 13 show similar results using the fully aberrated model of the lens for calculations. The absolute efficiencies are lower as expected, although still considerably higher than the experimental

values. The sensitivities to transverse displacements are significantly reduced in the y-direction while they are essentially unchanged in x. This is because only the wide far field angle in y samples the off-center regions of the GRIN lens where aberrations are most apparent. The coupling with respect to the longitudinal (i.e., z) fiber position also shows less sensitivity due to the spreading out of the effective focus point position by spherical aberration.

2.4 Coupling vs. Magnification

As discussed earlier, proper matching of the beam far field angles is important to high coupling efficiency and is achieved through the proper system magnification. For a given lens, the magnification is varied by changing the source to lens distance. Figure 14 shows the calculated coupling efficiency versus system magnification for a laser with far field angles of 40° and 25° FWHM and a fiber mode of 5.8° FWHM. Both the low and full aberration lenses are shown as well as a zero aberration curve based on Eqn. 3. While the optimum magnification is 5.2X, both lenses achieve maximum coupling at a magnification of about 3X due to increased aberration effects as the lens is used at higher magnification. The rather flat behavior of the aberrated lens results was also observed experimentally. Moderate changes in the laser-lens distance to increase the magnification resulted in very little change in coupling efficiency after reoptimizing the fiber position.

The low aberration lens shows near ideal performance for low magnification but quickly degrades for M>3. This points out that the

lens spherical aberration can only be optimized for a single magnification. Thus the laser-fiber combination must match the design magnification of the lens for optimum efficiency. While this can be achieved by designing any of the three elements-laser, lens, fiber-to match the other two, the most desirable choice in this case is to reduce the laser far field angles. This would then also reduce the aberration effects since the beam would be confined closer to the lens center. This is not a trivial task, however, since for the fiber and lens considered here, the laser must have a far field angle of about 18°.

3 References

[1] A. Yariv, *Quantum Electronics*, (Wiley, New York, 1975) p. 112

[2] J. W. Goodman, Introduction to Fourier Optics, (McGraw-Hill, San Francisco, 1968) p. 45

[3] D. Marcuse, Bell Syst. Tech. J. **56**, 703 (1977)

[4] H. Kogelnik, Symposium on Quasi-Optics, (Polytechnic Institute of Brooklyn, 1964) p. 333

[5] A. W. Snyder, IEEE Trans. Microwave Theory Tech., **MTT-17**, 1138 (1969)

[6] B. Hillerich, J. Lightwave Tech., **LT-7**, 77 (1989)

[7] M. Born and E. Wolf, Principles of Optics, (Pergamon Press, New York, 1980) p. 116

[8] N. S. K. Kwong, K. Y. Lau, N. Bar-Chaim, I. Ury, and K. J. Lee, Appl. Phys. Lett. **51**, 1879 (1987)

[9] I. Kitano, M. Toyama, and H. Nishi, Appl. Opt. **22**, 396 (1983)

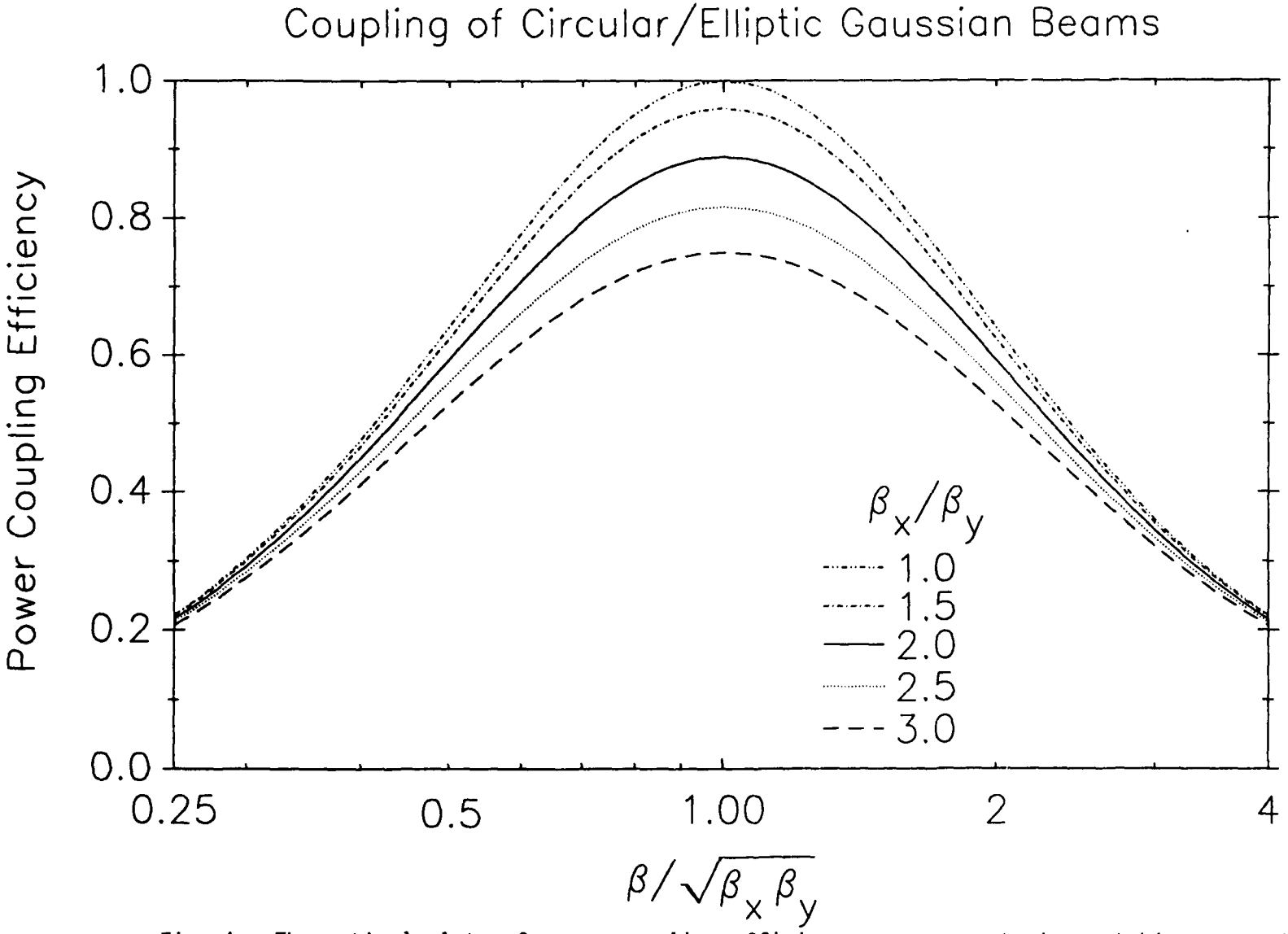

Fig. 1 Theoretical plots of power coupling efficiency versus spot size matching parameter for various degrees of ellipticity.

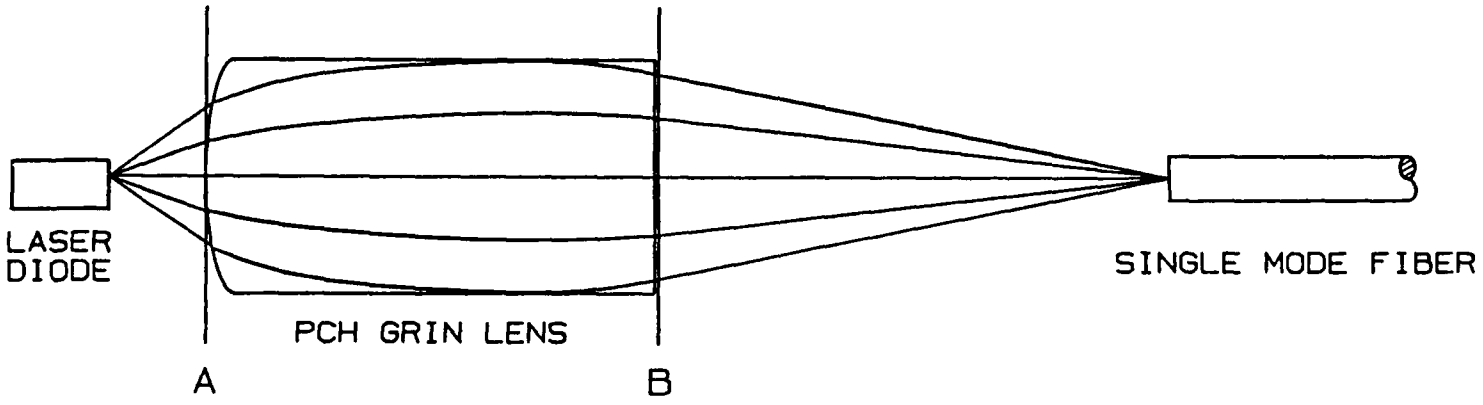

Fig. 2 A single graded index lens coupling system.

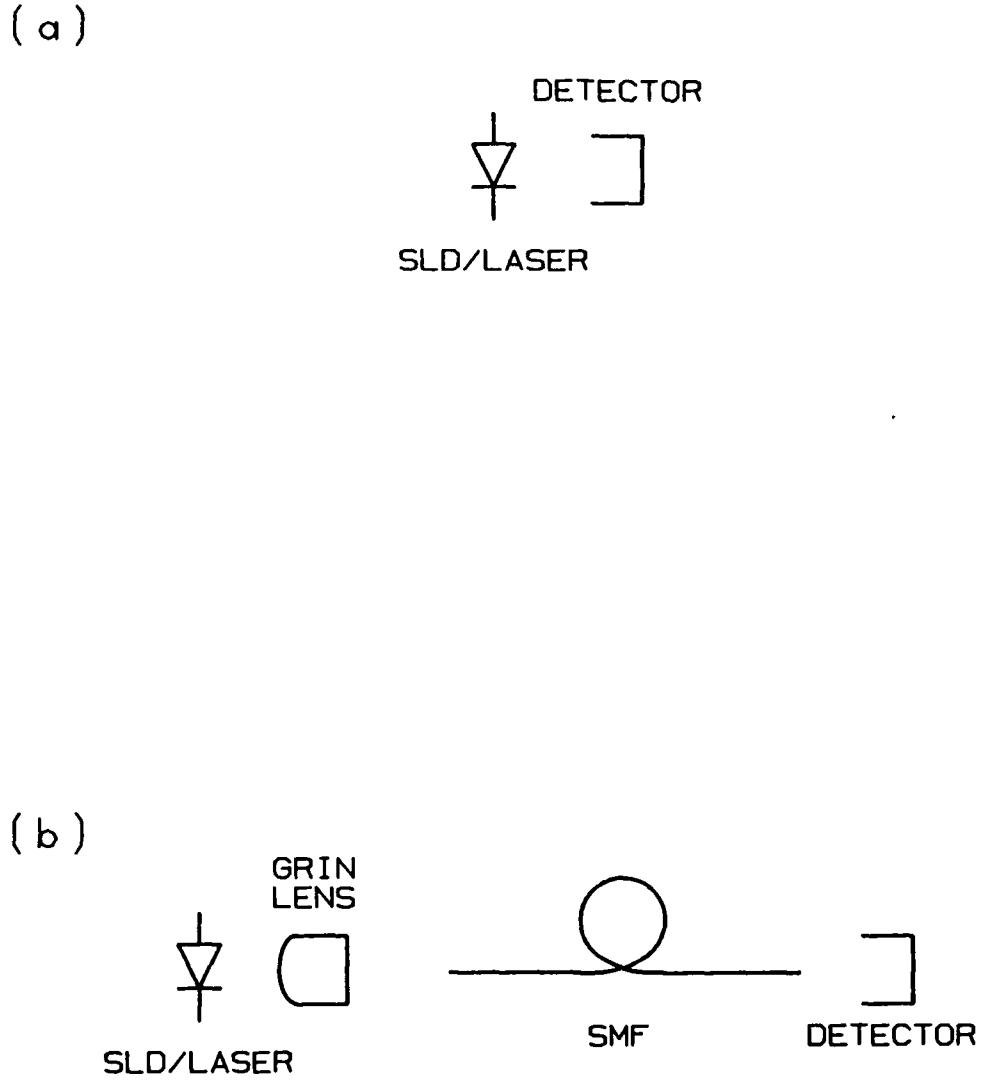

Fig. 3 Schematic diagram of experiment to measure the fiber coupling efficiency.

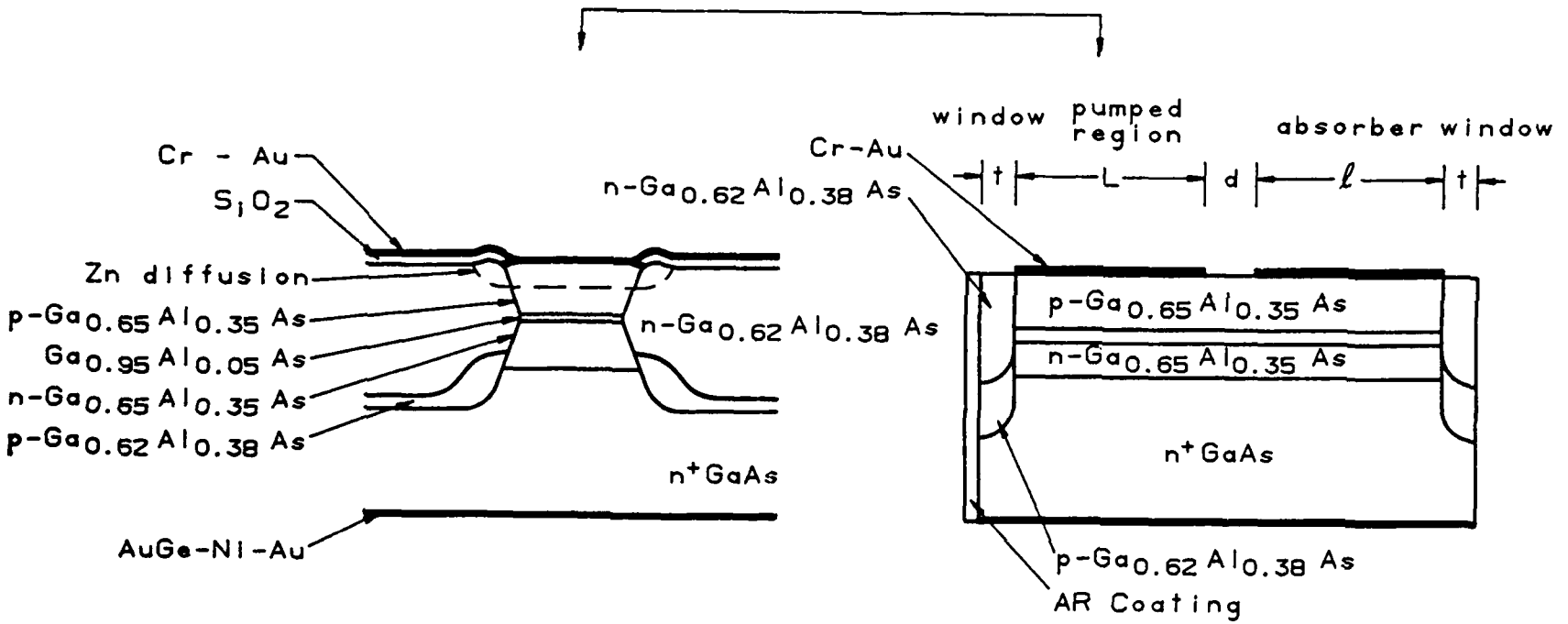

Fig. 4 Schematic diagram of GaAs Light source.

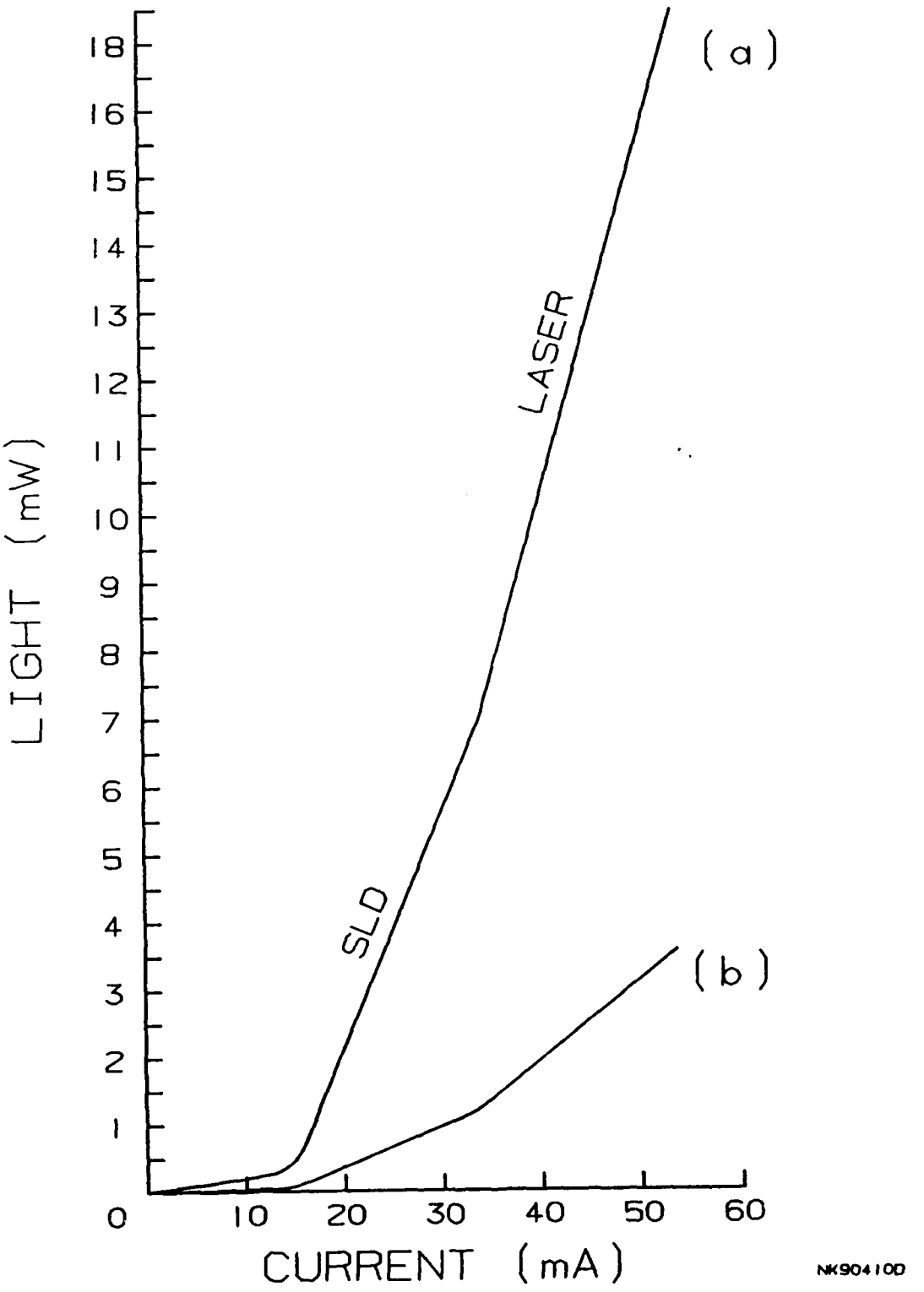

Fig. 5 Light versus current for the GaAs device.
(a) without fiber coupling
(b) power into single mode fiber

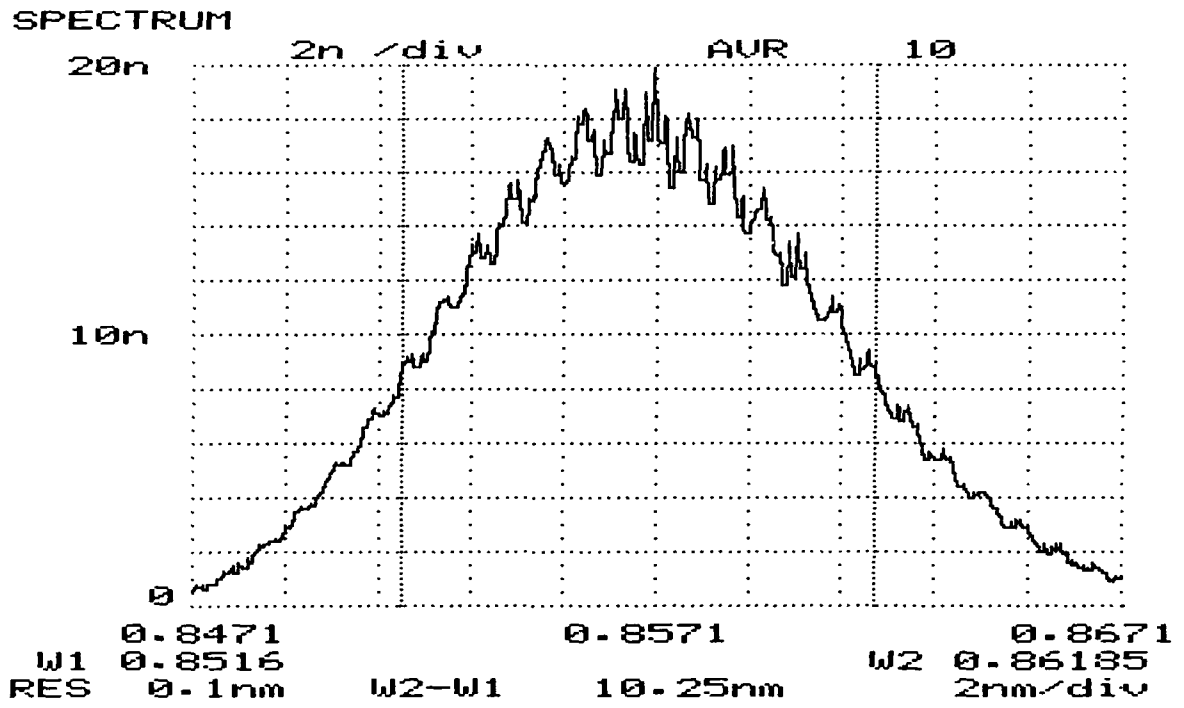

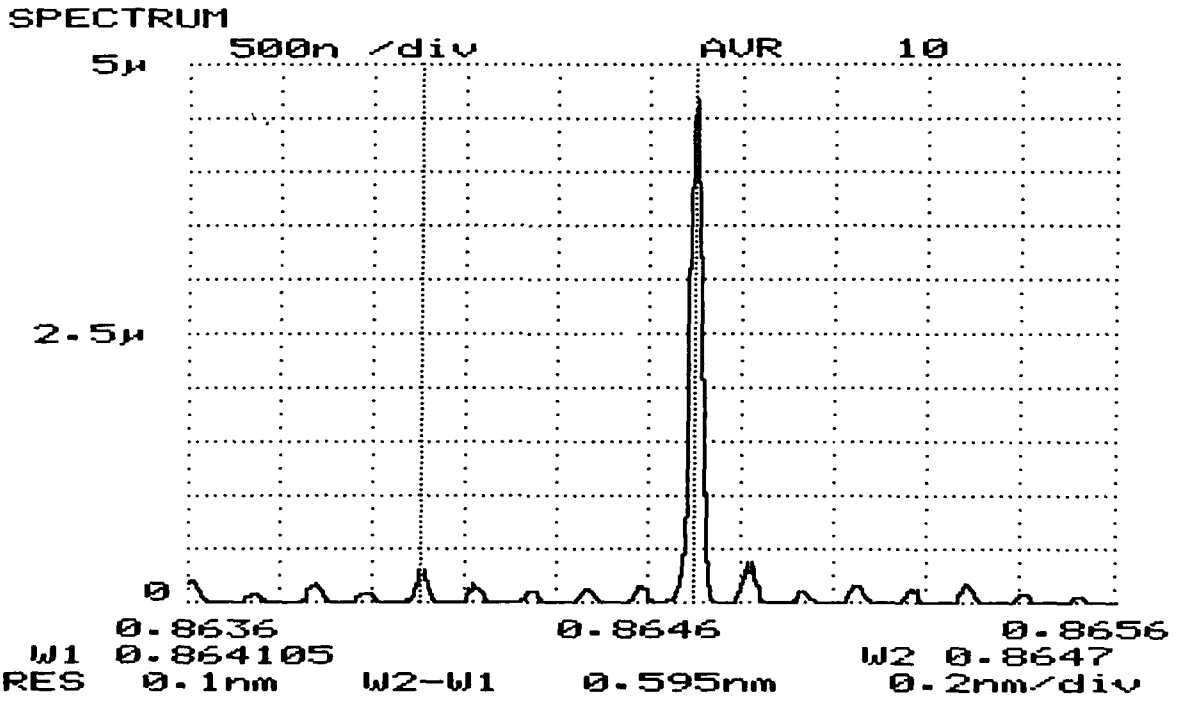

Fig. 6 Optical spectrum of the light source at
(a) 30 mA (SLD mode)
(b) 50 mA (Laser mode)

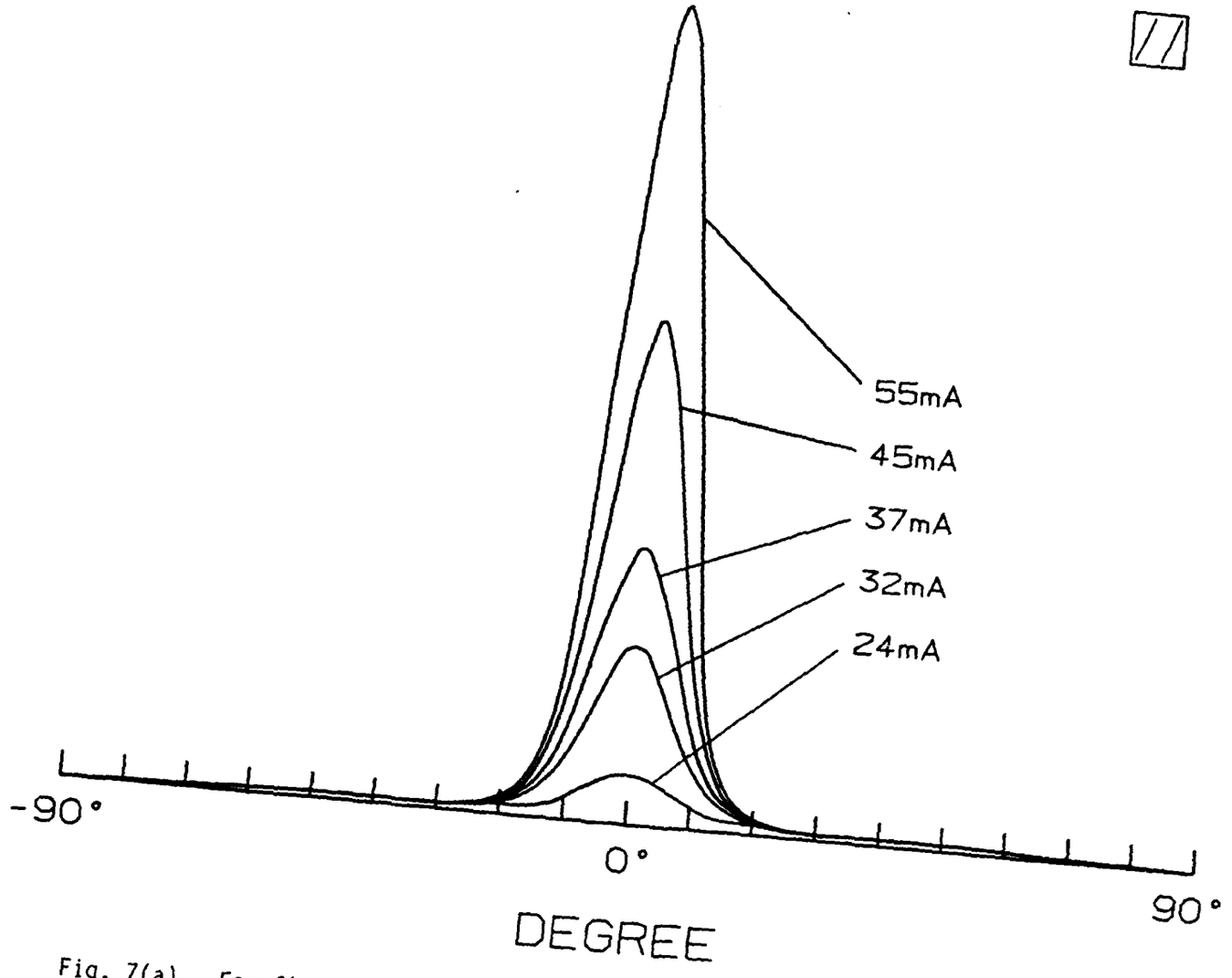

Fig. 7(a) Far-field pattern of the high source in the direction parallel to the junction plane.

NK904108

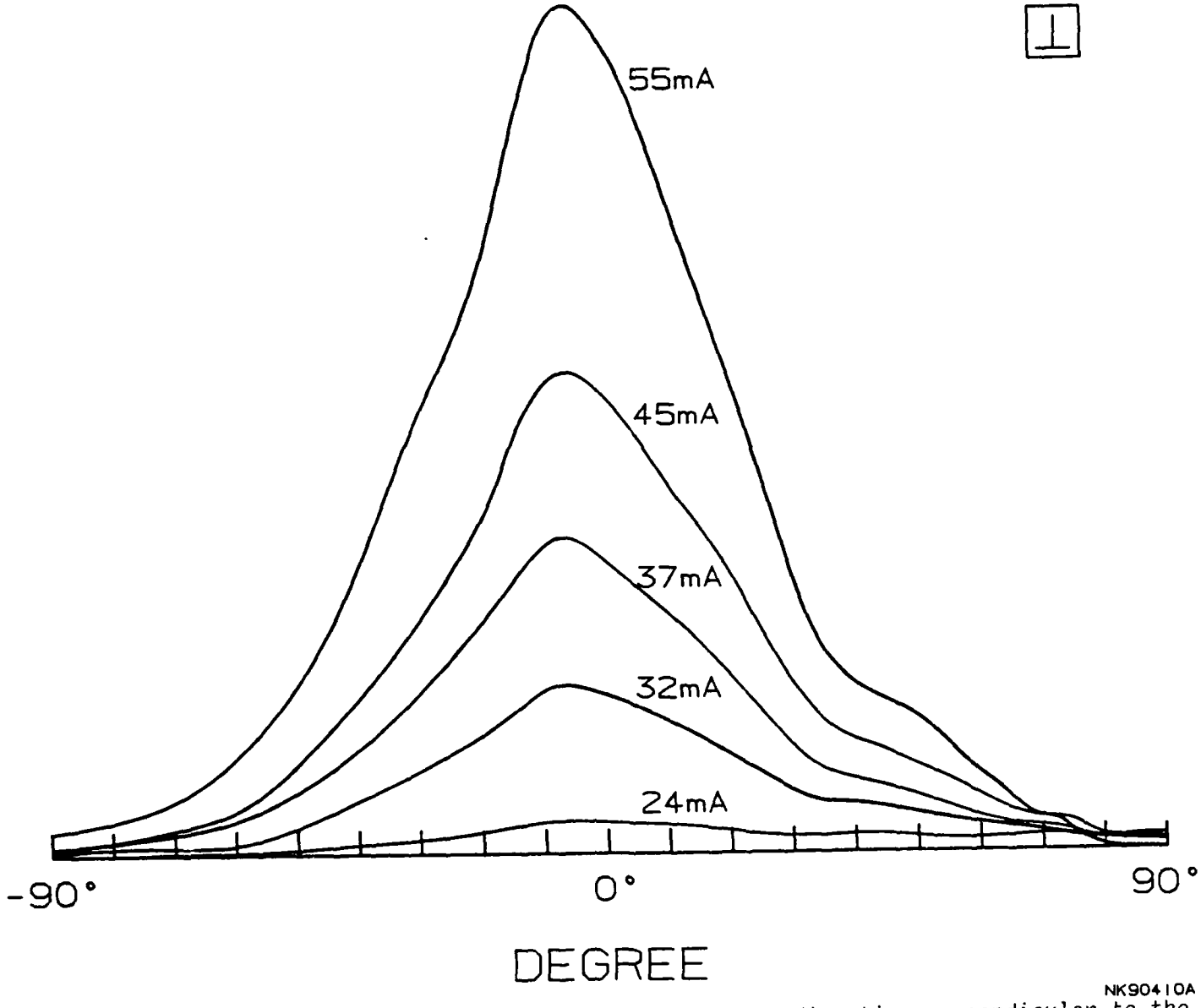

Fig. 7(b) Far-field pattern of the high source in the direction perpendicular to the junction plane.

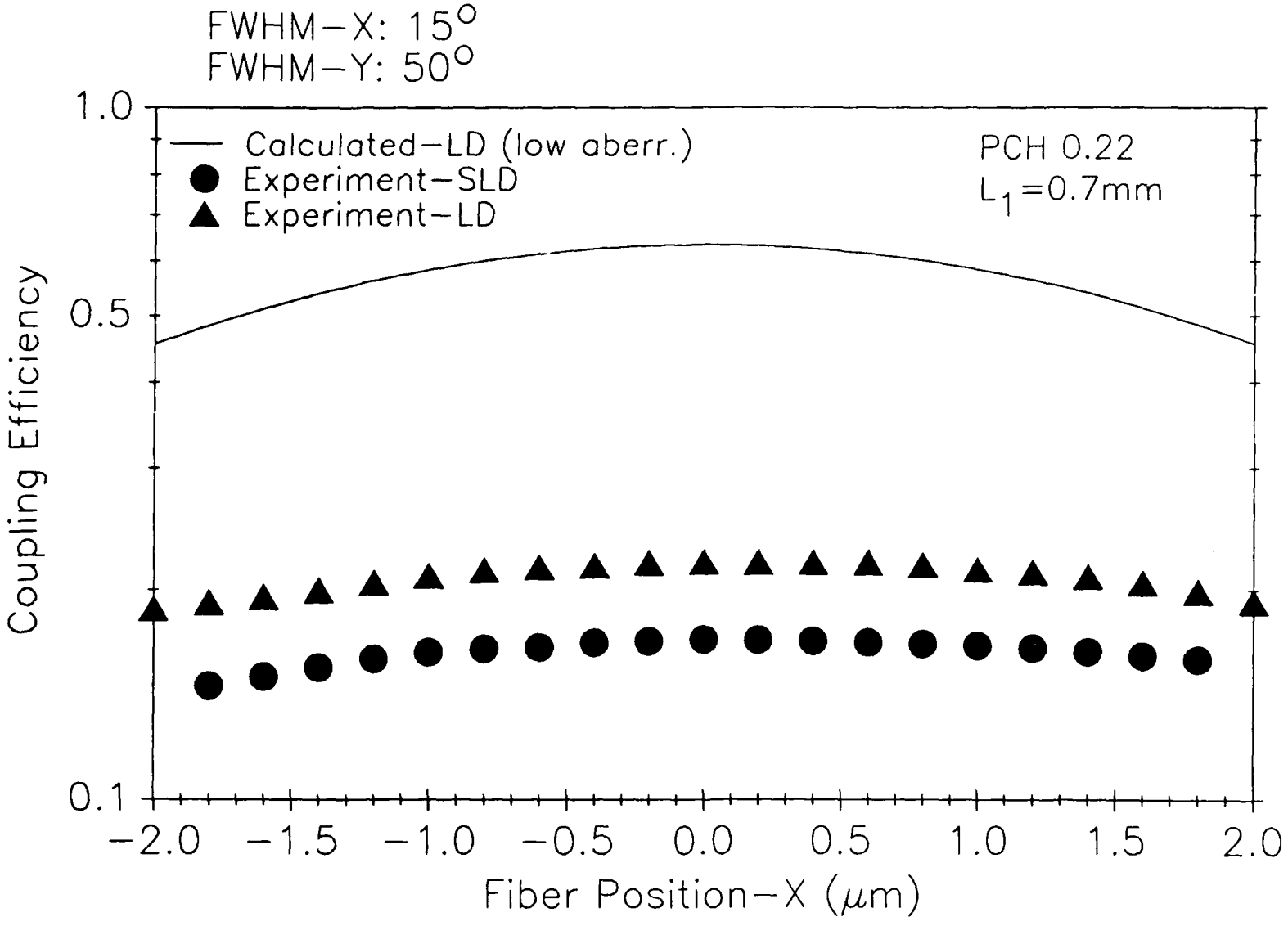

Fig. 8 Power coupling efficiency versus fiber position -X. (with low aberration)

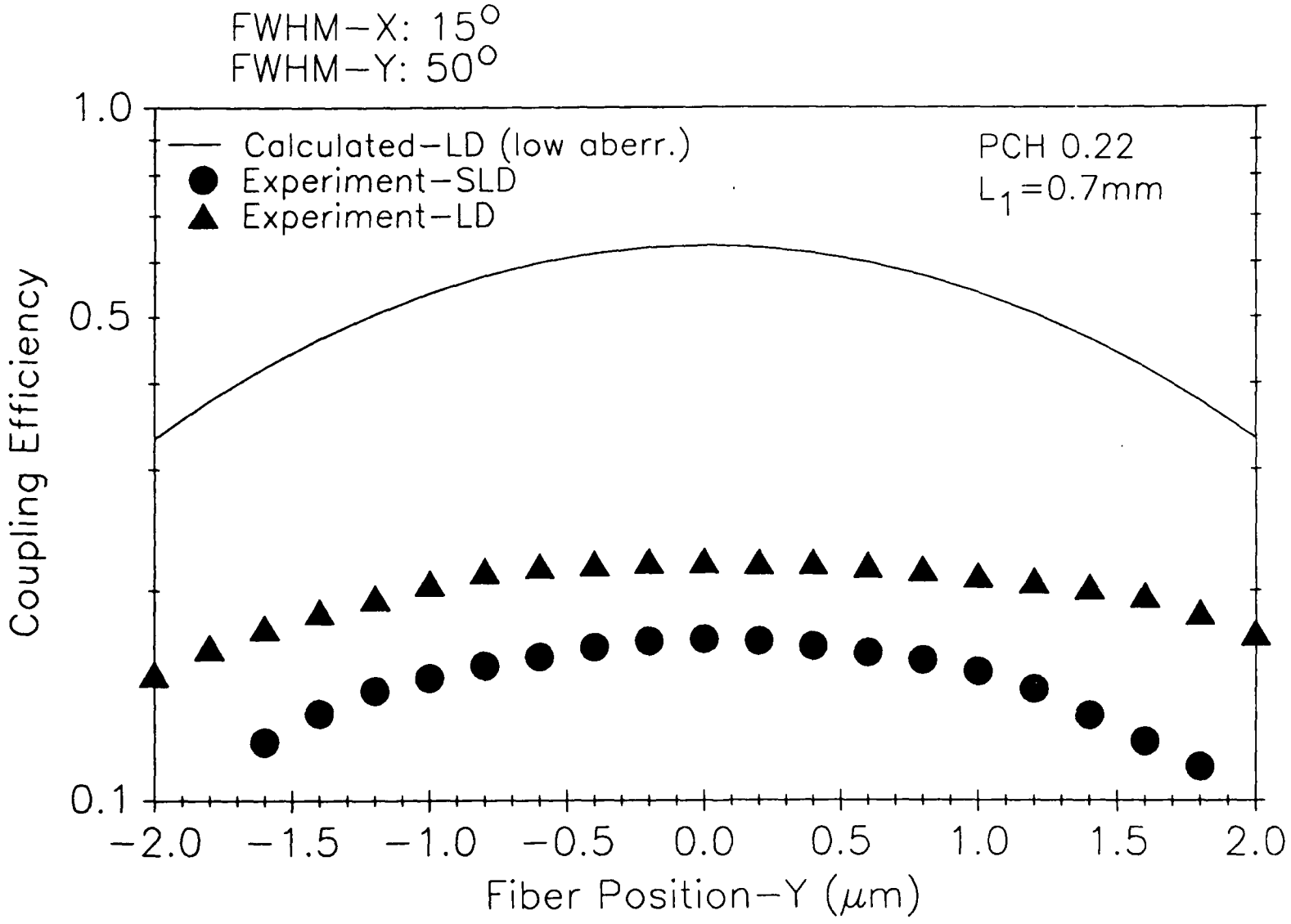

Fig. 9 Power Coupling efficiency versus fiber position -Y (with low aberration)

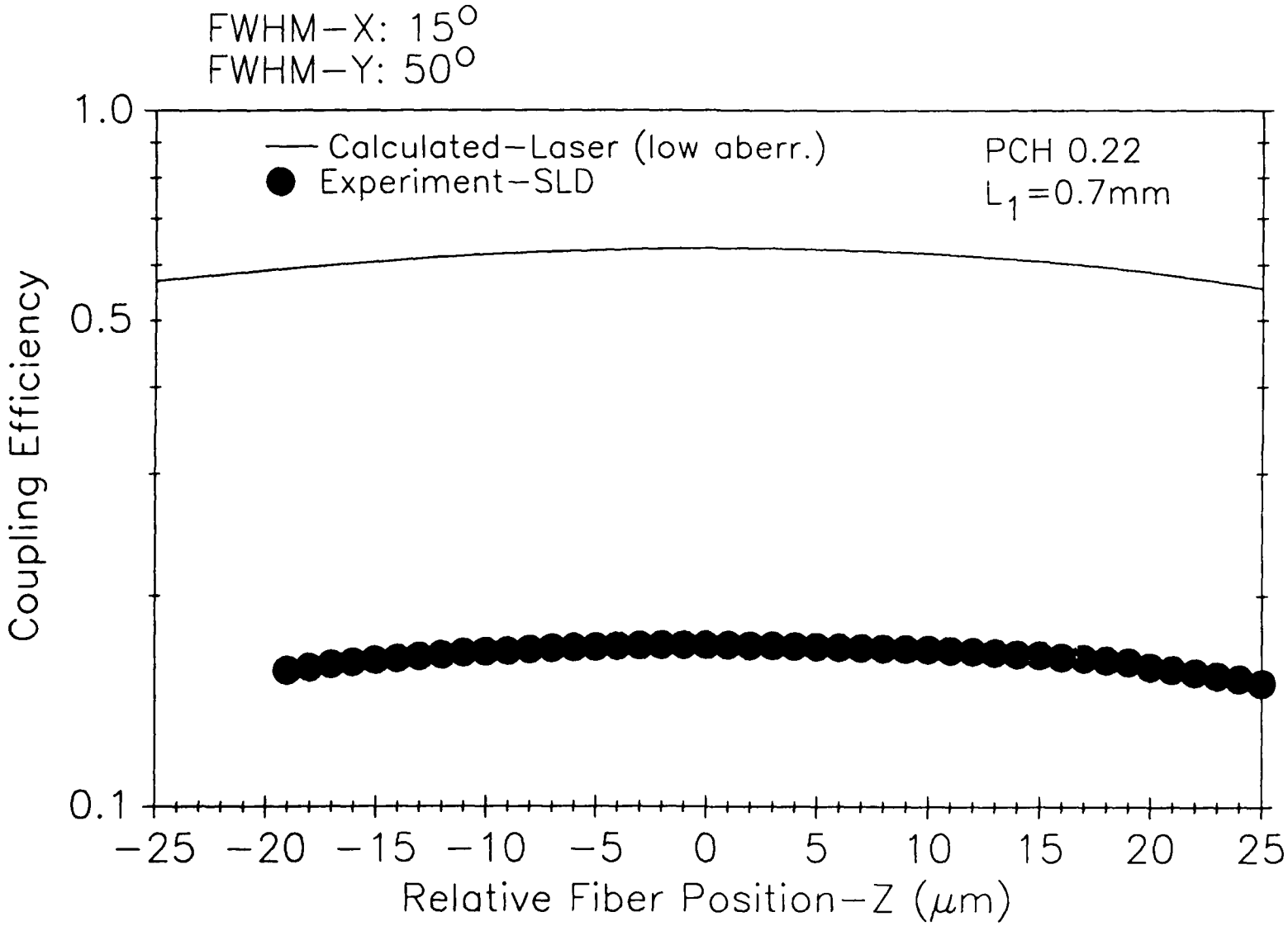

Fig. 10 Power coupling efficiency versus fiber position -Z. (with low aberration)

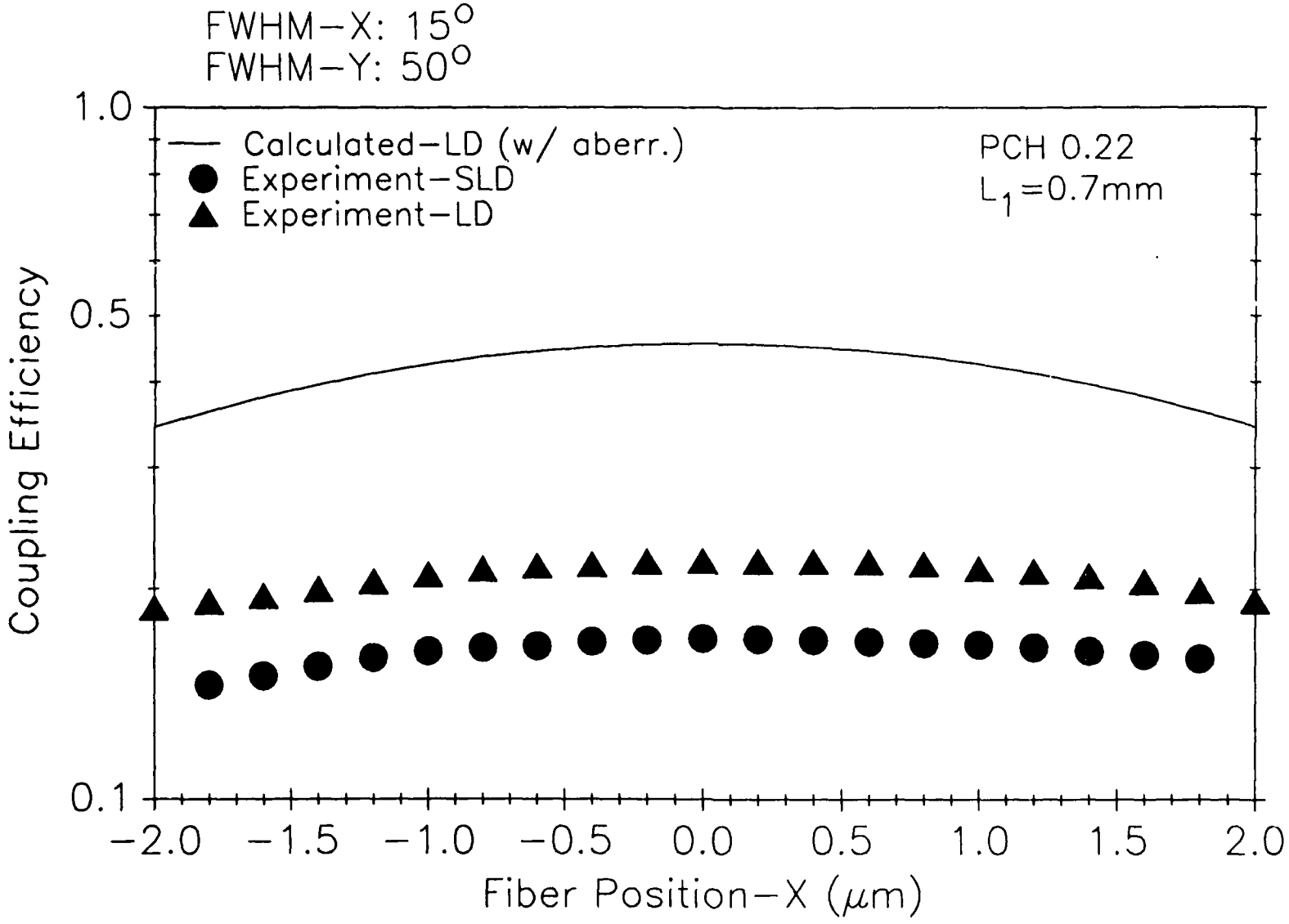

Fig. 11 Power Coupling efficiency versus fiber position -X. (with aberration)

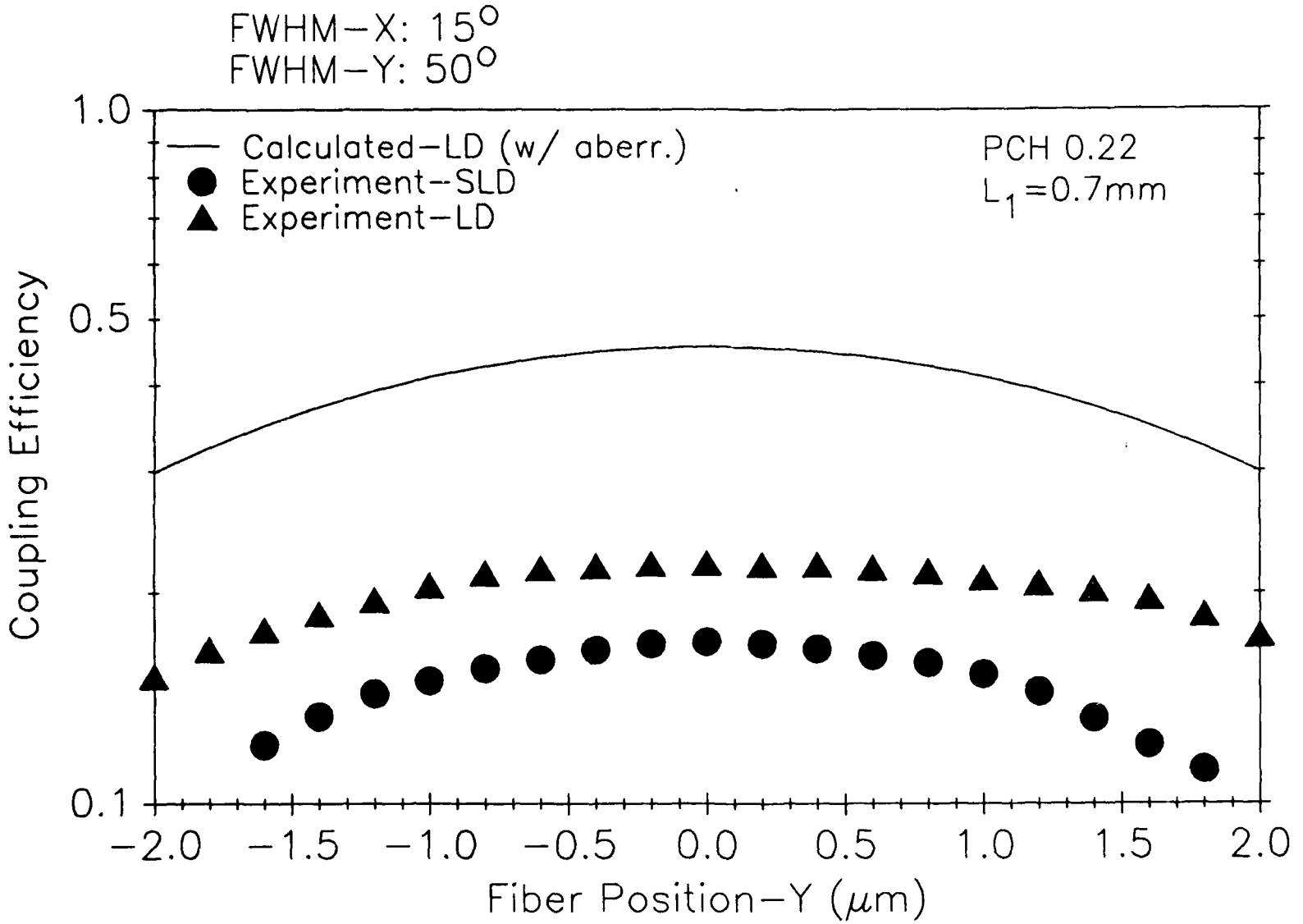

Fig. 12 Power coupling efficiency versus fiber position -Y. (with aberration)

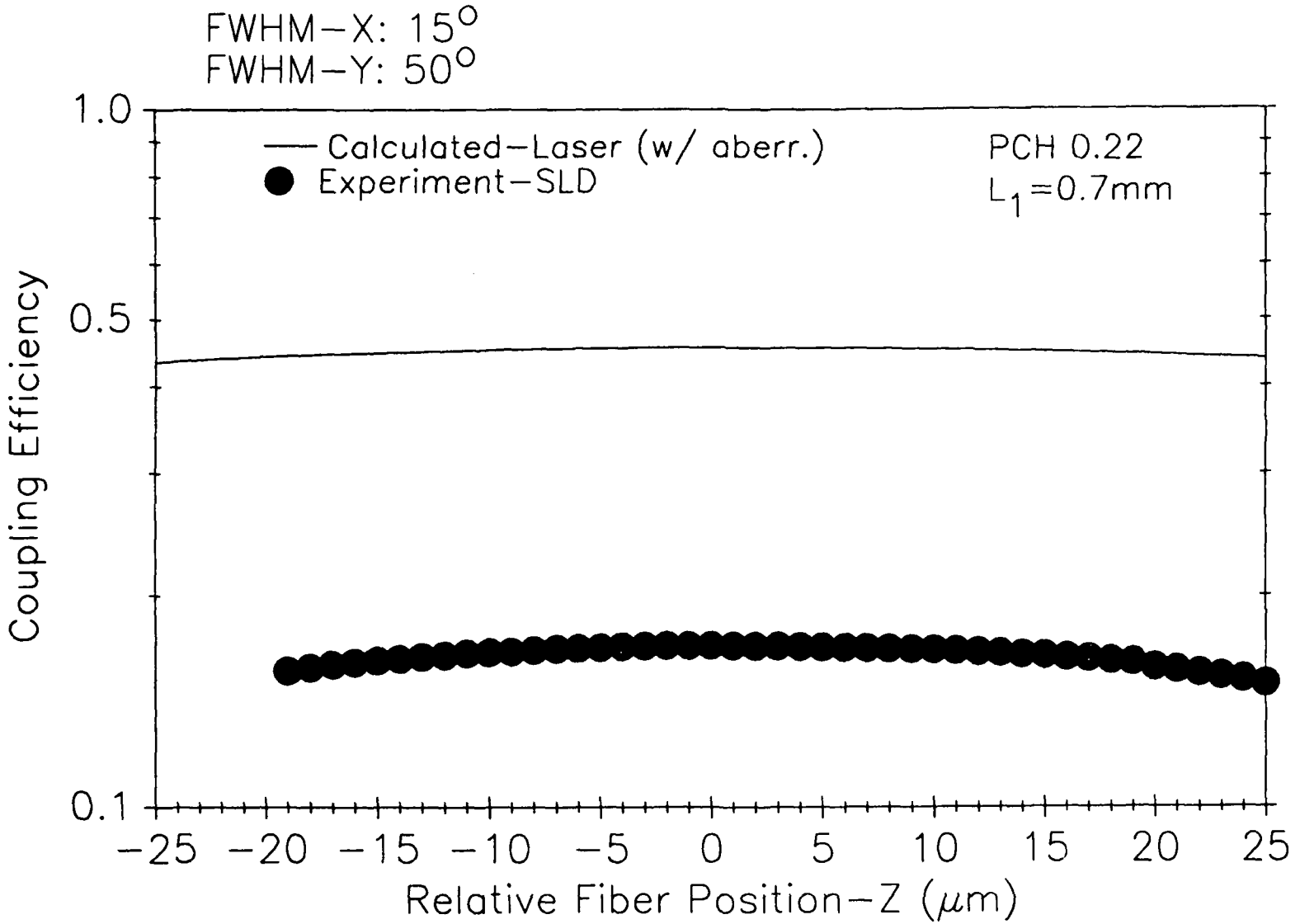

Fig. 13 Power coupling efficiency versus fiber position -Z. (with aberration)

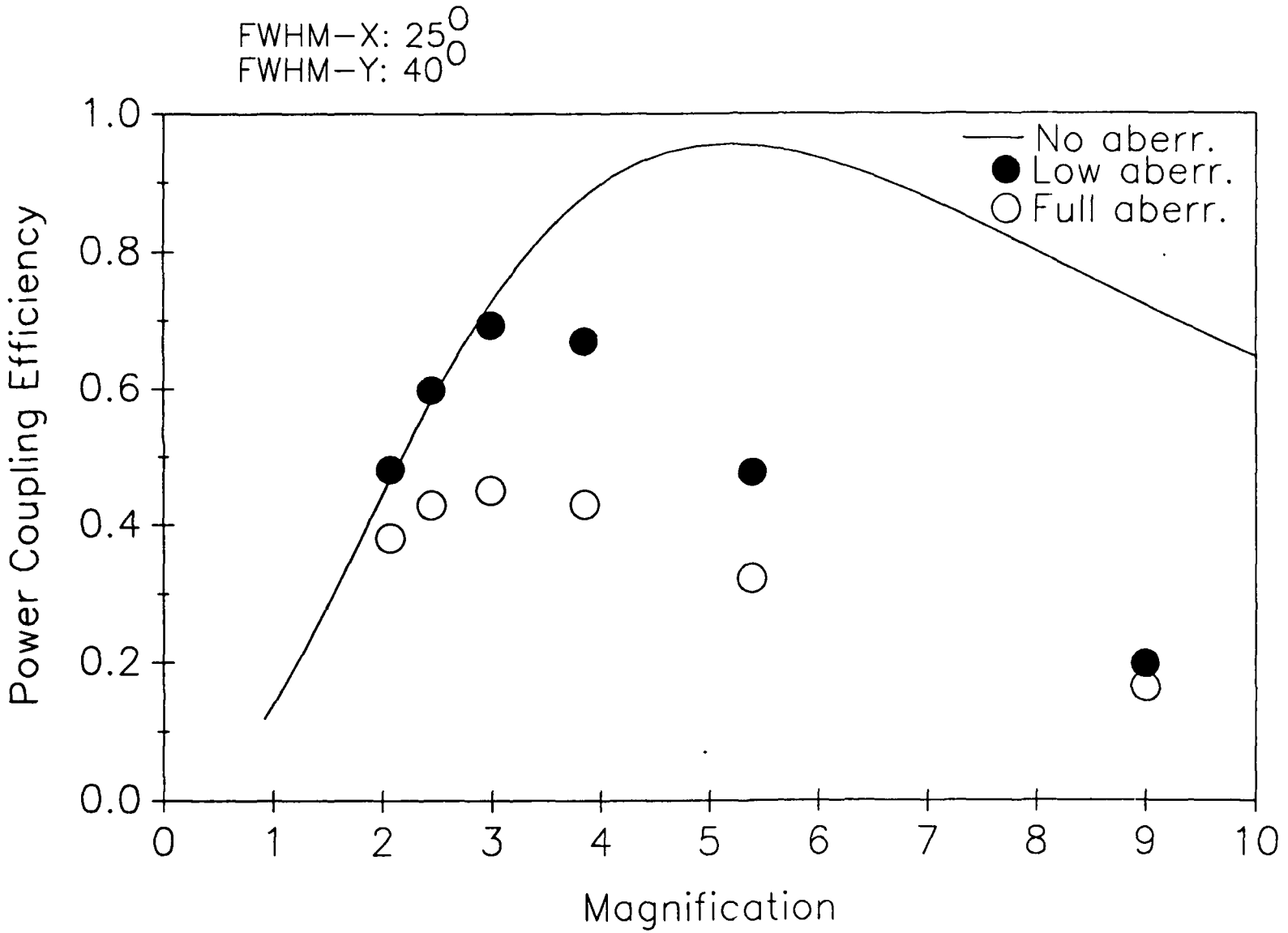

Fig. 14 Calculated coupling efficiency versus system magnification for a laser with far-field angles of 40° x 25° FWHM and fiber mode of 5.8° FWHM.

ORTEL™
CORPORATION

April 28, 1989

Mr. M. Musselman
Naval Research Laboratory
Code: 6503
4555 Overlook Avenue, S.W.
Washington, D.C. 20375-5000

Reference: Contract Number N00014-88-C-2033

Dear Mr. Musselman:

This letter certifies that the following hours were charged by labor category in completion of this contract:

Scientist	293 hours
Engineer	23 hours
Technician	10.5 hours

Very truly yours,

ORTEL CORPORATION

Peter J. Moerbeek
Vice President and Controller

PJM:dlk

2015 West Chestnut Street, Alhambra, California 91803 (818) 281-3636 Telex: 752434 Fax: (818) 281-8231